Microfluidics and Nanofluidics (2022) 26:6
https://doi.org/10.1007/s10404-021-02512-0

RESEARCH PAPER

Continuous separation of microparticles based on optically induced dielectrophoresis

Liuyong Shi[1] · Xiangtao Zhong[1] · Hanghang Ding[1] · Zhihang Yu[2] · Jing Jin[2] · Teng Zhou[1] · Yonggang Zhu[2] · Zhenyu Liu[3]

Received: 28 May 2021 / Accepted: 14 December 2021 / Published online: 5 January 2022

Abstract
To achieve high-throughput and high-efficiency separation based on optically induced dielectrophoresis (ODEP), an ODEP-based transient numerical model containing microparticles is developed under alternating current (AC) electric field coupling with an open flow field. In this model, the MST method is employed to calculate the time-averaged AC DEP force and the fluid viscous resistance acting on the particle, the Arbitrary Lagrangian–Eulerian (ALE) method is used to numerically solve the strong coupling electric-fluid–solid mechanics, and the efficient and continuous separation of microparticles is achieved. The results show that the trajectories of particles with different conductivity are clearly differentiated due to two different DEP actions, which enables separation of particles, and its separation performance can be optimized by adjusting the key parameters, including bright area width, applied alternating current (AC) electric voltage and inlet flow velocity. This study explains the continuous separation mechanism of particles under the combined action of AC electric field and flow field, and provides theoretical support for the design of high-efficiency ODEP microparticles separation device.

Keywords Optically induced dielectrophoresis (ODEP) · Arbitrary Lagrangian–Eulerian (ALE) · Microfluidics · Numerical simulation · Continuous separation

1 Introduction

The rapid separation and purification of biological particles is usually a prerequisite step in biochemical analysis and clinical medicine application, and it has attracted wide attention of researchers (Al-Faqheri et al. 2017; Antfolk and Laurell 2017; Shields et al. 2015; Tsou et al. 2020). For example, it is necessary to separate bacteria and parasitics in water quality monitoring (Porter et al. 1993). In clinical medical diagnosis, the primary problem is how to quickly and accurately separate target cells from samples (Lin et al. 2020). When analyzing and detecting biological bacteria, it is necessary to purify the bacteria to reach a certain concentration (Heinlaan et al. 2017). All of these rely on the separation technology of biological particles.

Traditional microparticles separation techniques including differential centrifugation, density gradient centrifugation, filtration, etc., are only suitable for large sample sizes (Shields et al. 2015). Flow cytometry can achieve high-precision cell separation, whereas it usually requires expensive and complex instruments operated by professional staff, as well as special reagents for cell marking (Galbraith 2012). Microfluidic chip, also known as Micro Total Analysis System (μ-TAS) or lab-on-a-chip, is suitable for the manipulation of biological microparticles due to its miniaturized size and good biocompatibility. Especially, dielectrophoresis (DEP) is a micro–nano-manipulation technology which is easy to be integrated into microfluidic chip (Butt and Wakeman 1997; Pethig and Markx 1997). Moreover, it has the merits of non-contact, non-damage and high throughput, and can be used to handle single or large numbers of particles (Yan et al. 2021; Zhao et al. 2014b). However, complex physical electrodes need to be designed and processed in traditional dielectrophoresis technology, which results in a

✉ Teng Zhou
zhouteng@hainanu.edu.cn

[1] Mechanical and Electrical Engineering College, Hainan University, Haikou 570228, China

[2] School of Mechanical Engineering and Automation, Harbin Institute of Technology (Shenzhen), Shenzhen 518055, China

[3] Fine Mechanics and Physics (CIOMP), Changchun Institute of Optics, Chinese Academy of Science, Changchun 130033, Jilin, China

few drawbacks including long design cycle and high cost, and also limits its flexibility in practical application.

Optically induced dielectrophoresis (ODEP) combines virtual electrodes formed by illuminating optical patterns onto photoconductive layers with DEP, and can carry out the manipulation of micro–nano objects (Chiou et al. 2005; Qu et al. 2012). By replacing physical electrodes with optical virtual electrodes, the complex electrode manufacturing process is simplified, the design cycle of a microfluidic chip is shortened and the processing cost is saved. In recent years, the ODEP has been widely applied in the capture, separation and assembly of polystyrene beads (Liang et al. 2013; Zhao et al. 2014a), cancer cells (Chiu et al. 2018; Chu et al. 2020), bacteria (Wang et al. 2020; Xie et al. 2017) and even drug-containing particles (Chen et al. 2019; Chu et al. 2019). Nevertheless, previous studies on ODEP technology generally manipulate a single or small batches of microparticles based on optical-induced dielectrophoresis force, and the flow field action is discarded, thus resulting in low separation efficiency.

In this study, to achieve efficient and continuous separation of microparticles, an ODEP-based transient numerical model including microparticles is constructed under alternating current (AC) electric field coupling with an open flow field. Maxwell stress tensor (MST) method is adopted to calculate the time-averaged AC DEP force and the fluid viscous resistance acting on the particle, which has been proved to be the most rigorous method for calculating DEP force, and can be used to explain the electric field distortion due to the presence of particles (Ai and Qian 2010; Wang et al. 1997). Arbitrary Lagrange–Euler (ALE) method combines Lagrange method to trace particles with Euler method to describe flow field, and it is especially suitable for dealing with mesh distortion (Al Quddus et al. 2008; Hu et al. 2001), so it is employed to numerically solve the strong coupling electric-fluid–solid mechanics issue. The continuous separation of microparticles is achieved by introducing the open flow field, which dramatically reduces the dwelling time of particles in the microchannel and has a significant effect on improving the particle separation efficiency. To optimize the continuous separation performance of microparticles, several critical parameters including the width of bright area, applied electric voltage and inlet flow rate on particles movement and separation effect are discussed in positive DEP and negative DEP cases, respectively.

2 Theory

2.1 Mathematical model and parameters

ODEP chips are generally sandwich structures: the middle microchannel layer is sandwiched by the upper and lower indium tin oxide (ITO) conductive glass wall. The photoconductive layer with multilayer structure is deposited on the lower ITO glass by plasma enhanced chemical vapor deposition (PECVD), which is from bottom to top as follows: heavy-doped hydrogenated amorphous silicon ($n^+\alpha$-Si:H) layer for reducing contact resistance between substrate and intrinsic hydrogenated amorphous silicon (α-Si:H), α-Si:H layer (forming photoconductive reaction area) and nitride insulator (preventing hydrolysis at low frequency and high-voltage condition) (Chiou et al. 2005). The two-dimensional structure of the physical model based on the above ODEP chip structure is shown in Fig. 1. A circular particle with a diameter of d_P moves in a rectangular microchannel CDEF

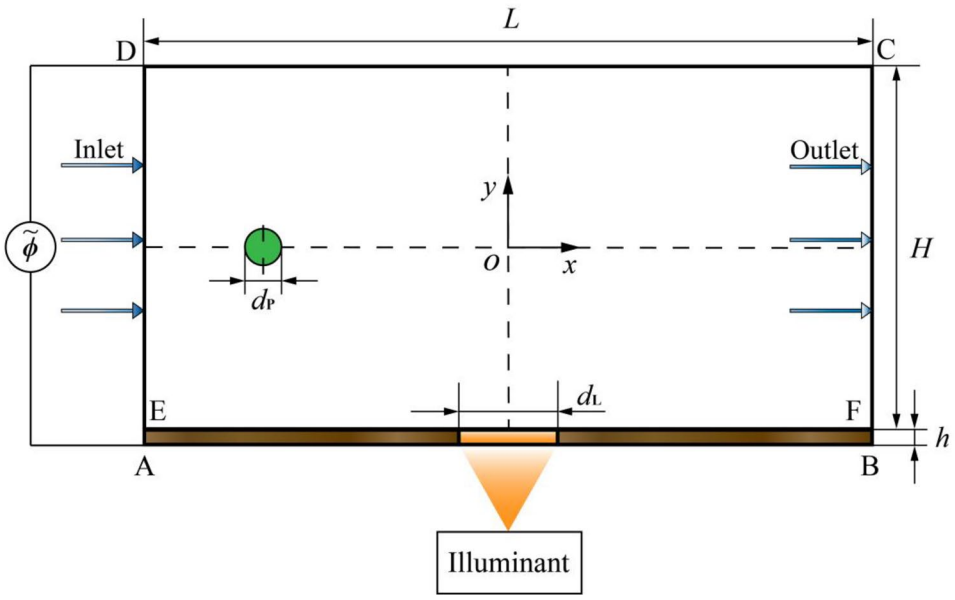

Fig. 1 A two-dimensional structural schematic diagram of ODEP chip containing single circular particle moving in a rectangular microchannel. The *xoy* coordinate system is established in the center of the whole microchannel. The left and the right arrows represent the fluid inlet and the fluid outlet, respectively. The green circle represents the microparticle. The brown and orange areas at the bottom of the microchannel represent the photoconductive layer, in which the orange area represents the area under light (bright area), and the rest of area represents the area without light (dark area)

with the length of L and the height of H, which is filled with a fluid medium. The region ABFE is a photoconductive layer with the length of L and the height of h. It is worth noting only the α-Si:H layer related to the formation of the photoconductive reaction area is included in this model, and the other two layers are ignored. The center point O of the region CDEF is selected as the origin of the two-dimensional Cartesian coordinate system xoy. AC potential is applied to the bottom boundary AB and the top boundary CD, which represents the ITO thin-film electrodes. The boundary DE is set as the inlet of the fluid, and the corresponding outlet is the boundary CF. Due to the illumination of the bottom light source, a bright area with a diameter of d_L is generated in the photoconductive layer.

When the particle is placed in the microchannel, it will be subjected to DEP force due to the non-uniform electric field, which is generated by the vastly varying conductivity of the bright and dark regions. Considering that the DEP force is related to the real part of the Clausius–Mossotti (CM) factor, which depends on the complex permittivity of particles and fluid media:

$$K(\omega) = \frac{\widetilde{\varepsilon_P} - \widetilde{\varepsilon_F}}{\widetilde{\varepsilon_P} + 2\widetilde{\varepsilon_F}}, \tag{1}$$

where $K(\omega)$ represents the real part of the CM factor, ω is the angular frequency of the applied AC electric field, the superscript "~" represents a complex variable, $\widetilde{\varepsilon_P}$ and $\widetilde{\varepsilon_F}$ represents the complex permittivity of particles and fluid media, respectively:

$$\widetilde{\varepsilon} = \varepsilon - i\sigma/\omega, \tag{2}$$

where ε represents permittivity, σ represents conductivity, $i=\sqrt{-1}$ is an imaginary unit.

In Eq. (1), positive DEP action is denoted when the real part of CM factor is a positive value, and negative DEP action is implied when it is a negative value. As shown in Fig. 2, on the premise that all other parameters except the particle conductivity are consistent, the different DEP actions may be generated at the same frequency due to the varying particle conductivity. Based on this, particles separation can be achieved.

The employed parameters are set as follows: The length of the microchannel and photoconductive layer is $L=200$ μm, the height of microchannel is $H=100$ μm, the thickness of photoconductive layer made of α-Si:H is $h=2$ μm, the diameter of the particle is $d_P=10$ μm, and the width of the bright area is $d_L=30$ μm. Rectangular microchannels are filled with deionized aqueous solutions as fluid media. Density, dynamic viscosity, conductivity and relative dielectric constants of fluid are $\rho_F=1\times10^3$ kg/m^3,$\mu=1\times10^{-3}$ Pa · s ,$\sigma_F=1\times10^{-3}$ S/m and $\varepsilon_F=80$, respectively. Fluid flows from boundary DE at a velocity of $V_{inlet}=1$ mm/s and the initial velocity of the particle is $u^*=0$. Density and shear modulus of polystyrene particles are $\rho_P=1.05\times10^3$ S/m and $G_P=10^9$ Pa, respectively. The relative dielectric constant of the particle is ε_P=2.6, the particle conductivity $\sigma_{P1}=4\times10^{-2}$ S/m and $\sigma_{P2}=4\times10^{-4}$ S/m are selected to generating positive and negative DEP action, respectively. Relative permittivity of photoconductive layer, conductivity in bright area and conductivity in dark area are ε_S=11.7, $\sigma_L=2\times10^{-1}$ S/m and $\sigma_D=6.7\times10^{-5}$ S/m, respectively. The frequency and voltage peak values of the applied AC electric field are $f=1$ MHz and ϕ_0=30V, respectively.

2.2 Governing equations and boundary conditions

To simplify the calculation, the dimensionless method commonly used in hydrodynamics calculation is adopted in this study. The selected characteristic length, characteristic potential and characteristic velocity are $a=d_P/2=5$ μm, $\phi_\infty=R_0T/F$ and $U_\infty=(\varepsilon_F\phi_\infty^2)/(\eta a)$, respectively, where

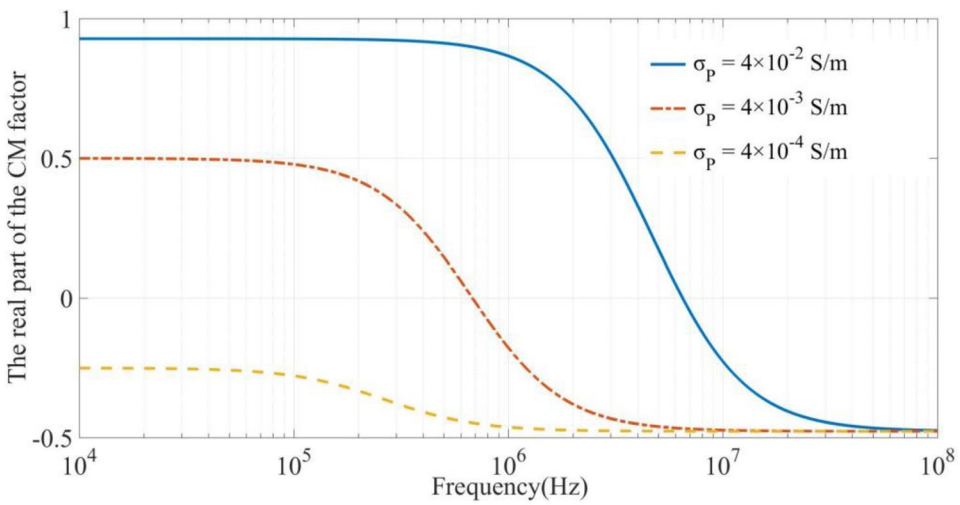

Fig. 2 The relationship between the real part of CM factor and the electric field frequency under three kinds conductivity of particles ($\sigma_P=4\times10^{-2}$ S/m, 4×10^{-3} S/m, 4×10^{-4} S/m) and the fluid medium conductivity ($\sigma_F=1\times10^{-3}$ S/m), the relative dielectric constant of the fluid medium (ε_F=80) and the relative dielectric constant of particles (ε_P= 2.6)

R_0 is the universal gas constant, $T = 300$ K is the absolute temperature of the fluid medium, and F is the Faraday constant. Then the following basic physical quantities can be obtained:

$$\mathbf{S} = a\mathbf{S}^*,\ \mathbf{u} = U_\infty \mathbf{u}^*,\ p = \mu U_\infty p^*/a,$$

$$\widetilde{\phi} = \phi_\infty \widetilde{\phi^*},\ t = at^*/U_\infty \ \mathrm{Re} = \rho_\mathrm{F} a U_\infty/\mu,$$

where, $\mathbf{S}$ is the displacement of the particle, $\mathbf{u}$ is the velocity vector of fluid, p is the pressure, μ is the dynamic viscosity, $\tilde{\phi}$ is electric potential, t is time, Re is the Reynolds number, ρ_F is the density of fluid, respectively. The superscript "*" denotes a dimensionless variable.

Considering that the characteristic length of the model is much larger than the thickness of the electric double layer (EDL), the thin EDL assumption is tenable, the net charge density in the whole computational domain is zero. Moreover, the characteristic size of the model is much smaller than the electromagnetic wavelength; thus, the AC electric field can be regarded as a quasi-static electric field. Therefore, the distribution of the quasi-static electric field is governed by Gauss law, as follows:

$$\nabla^* \cdot (\widetilde{\varepsilon_\mathrm{F}^*} \nabla^* \widetilde{\phi_\mathrm{F}^*}) = 0 \quad \text{in } \Omega_\mathrm{F}, \tag{3}$$

$$\nabla^* \cdot (\widetilde{\varepsilon_\mathrm{P}^*} \nabla^* \widetilde{\phi_\mathrm{P}^*}) = 0 \quad \text{in } \Omega_\mathrm{P}, \tag{4}$$

$$\nabla^* \cdot (\widetilde{\varepsilon_\mathrm{D}^*} \nabla^* \widetilde{\phi_\mathrm{D}^*}) = 0 \quad \text{in } \Omega_\mathrm{D}, \tag{5}$$

$$\nabla^* \cdot (\widetilde{\varepsilon_\mathrm{L}^*} \nabla^* \widetilde{\phi_\mathrm{L}^*}) = 0 \quad \text{in } \Omega_\mathrm{L}, \tag{6}$$

where, the complex permittivity of fluid medium, particle, bright and dark areas are $\widetilde{\varepsilon_\mathrm{F}^*} = 1 - i\sigma_\mathrm{F}/(\omega\varepsilon_\mathrm{F})$, $\widetilde{\varepsilon_\mathrm{P}^*} = 1 - i\sigma_\mathrm{P}/(\omega\varepsilon_\mathrm{P})$, $\widetilde{\varepsilon_\mathrm{L}^*} = 1 - i\sigma_\mathrm{L}/(\omega\varepsilon_\mathrm{L})$ and $\widetilde{\varepsilon_\mathrm{D}^*} = 1 - i\sigma_\mathrm{D}/(\omega\varepsilon_\mathrm{D})$, respectively. The complex electric potentials of fluid media, particle, bright and dark areas are $\widetilde{\phi_\mathrm{F}^*}$, $\widetilde{\phi_\mathrm{P}^*}$, $\widetilde{\phi_\mathrm{L}^*}$ and $\widetilde{\phi_\mathrm{D}^*}$, respectively. The angular frequency of the applied AC electric field is $\omega = 2\pi f$. Ω_F, Ω_P, Ω_D and Ω_L represents the fluid medium domain (corresponds to the region CDEF), the particle domain (the green circular area), the bright and dark domains (the region ABFE), respectively.

The dimensionless boundary conditions corresponding to electric field are as follows:

$$\widetilde{\phi_\mathrm{F}^*} = \phi_0/\phi_\infty \quad \text{on AB and } \widetilde{\phi_\mathrm{F}^*} = 0 \text{ on CD}, \tag{7}$$

$$n \cdot \widetilde{\varepsilon_\mathrm{F}^*} \nabla^* \widetilde{\phi_\mathrm{F}^*} = 0 \quad \text{on AD and BC}, \tag{8}$$

where n denotes the unit normal vector on the corresponding boundary.

To ensure that electric potential and the normal component of electric displacement is continuous at the interface between fluid media and particle, the equations are as follows:

$$\widetilde{\phi_\mathrm{F}^*} = \widetilde{\phi_\mathrm{P}^*} \quad \text{on } \Lambda, \tag{9}$$

$$n \cdot \nabla^* \widetilde{\phi_\mathrm{F}^*} = \frac{\widetilde{\varepsilon_\mathrm{P}^*}}{\widetilde{\varepsilon_\mathrm{F}^*}} n \cdot \nabla^* \widetilde{\phi_\mathrm{P}^*} \quad \text{on } \Lambda, \tag{10}$$

where, Λ denotes the surface of the particle.

The continuity and Stokes equations are used to describe the fluid medium. Considering that the Reynolds number is minimal, the inertia term in the equation can be neglected. In the whole calculation process, the boundary DE is set as the inlet of the fluid medium, the boundary CF is set as the outlet of the fluid medium with zero pressure, and the boundary CD and EF are set as the wall boundary without sliding, expressed as:

$$\nabla^* \cdot \mathbf{u}^* = 0 \quad \text{in } \Omega_\mathrm{F}, \tag{11}$$

$$\mathrm{Re} \frac{\partial \mathbf{u}^*}{\partial t^*} = -\nabla^* p^* + \nabla^{*2} \mathbf{u}^* \quad \text{in } \Omega_\mathrm{F}. \tag{12}$$

In this study, the particle is defined as a circular rigid body. Since the particle density is close to that of deionized water solution, it can be considered that the gravity and buoyancy of particles offset each other. In addition, considering that the particle size used here is at a micron scale, the effect of Brownian motion on the particle can also be neglected. Therefore, only the time-averaged DEP force and the fluid viscosity resistance act on the particle. These two forces can be obtained by integrating the Maxwell stress tensor $\mathbf{T}_\mathrm{M}$ and the hydrodynamic stress tensor $\mathbf{T}_\mathrm{H}$ over the surface of the particle. So the time-averaged DEP force $\mathbf{F}_\mathrm{DEP}$ on the particle surface and the hydrodynamic force $\mathbf{F}_\mathrm{H}$ can be expressed as:

$$\mathbf{F}_\mathrm{DEP}^* = \int \mathbf{T}_\mathrm{M} \cdot \mathbf{n} d\Lambda^* = \int \frac{1}{4} [(\widetilde{\mathbf{E}^*}\widetilde{\mathbf{E}^*} + \widetilde{\mathbf{E}'^*}\widetilde{\mathbf{E}^*}) - |\widetilde{\mathbf{E}^*}|^2 \mathbf{I}] \cdot \mathbf{n} d\Lambda^*, \tag{13}$$

$$\mathbf{F}_\mathrm{H}^* = \int \mathbf{T}_\mathrm{H} \cdot \mathbf{n} d\Lambda^* = \int [-p^* \mathbf{I} + (\nabla^* \mathbf{u}^* + (\nabla^* \mathbf{u}^*)^T)] \cdot \mathbf{n} d\Lambda^*, \tag{14}$$

where, $\mathbf{F} = \eta U_\infty \mathbf{F}^*$, $\mathbf{T}^* = \eta U_\infty \mathbf{T}^*/a$, $\widetilde{\mathbf{E}^*}$ denotes electric field intensity, and $\mathbf{E}^* = -\nabla\widetilde{\phi^*}$, $\mathbf{E}'^*$ is the complex conjugate of $\widetilde{\mathbf{E}^*}$, $\mathbf{I}$ denotes the unit tensor.

Considering that the particle used here is a rigid circular particle, so its rotational motion can be neglected. Therefore, the velocity of a particle can be described as:

$$\mathbf{u}_{\mathrm{P}}^{*}=\frac{\varepsilon_{\mathrm{F}}^{*}\zeta_{\mathrm{P}}^{*}}{\mu^{*}}(\mathbf{I}-\mathbf{nn})\cdot\nabla^{*}\phi^{*}+\frac{\partial\mathbf{S}^{*}}{\partial t^{*}}\quad\text{on }\Lambda, \tag{15}$$

where, the first part on the right side of the equation is the slip velocity of electroosmotic flow, here the value of this item is set to zero since the electroosmotic flow is offset under the action of high frequency alternating current electric field, ζ_{P}^{*} denotes the zeta potential. In the latter part, $\mathbf{S}^{*}$ represents the displacement of the particle and can be derived from the following equation:

$$\mathrm{Re}\frac{\partial^{2}\mathbf{S}^{*}}{\partial^{2}t^{*}}-\nabla^{*}\cdot\boldsymbol{\sigma}(\mathbf{S}^{*})=0\quad\text{on }\Lambda, \tag{16}$$

where, $\boldsymbol{\sigma}(\mathbf{S}^{*})$ denotes the Cauchy stress of the solid particle, and it is a function of the displacement of the particle. Consider the hyperelastic particle as an incompressible neo-Hookean material that could be mathematically described using the strain energy density function:

$$W=G_{\mathrm{P}}\left(I_{c}-3\right)/2, \tag{17}$$

here, G_{P} is the particle's shear modulus, $I_C = tr(C)$ is the first invariant of the right Cauchy–Green tensor, given by $C=\mathbf{F}^{*\mathrm{T}}\mathbf{F}^{*}$, $\mathbf{F}^{*}=\nabla_{\mathrm{X}}^{*}\mathbf{S}^{*}+\mathbf{I}$ is the deformation gradient tensor with X denoting the reference position, $\boldsymbol{\sigma}(\mathbf{S}^{*})=\mathbf{P}^{*}\mathbf{F}^{*T}$, $\mathbf{P}^{*}=\partial W/\partial\nabla_{\mathrm{X}}^{*}\mathbf{S}^{*}$ is the first Piola–Kirchhoff stress.

2.3 Implementation of the model

In this study, the ALE method was used to solve the strong coupling electric field-fluid field-solid mechanics numerically. The commercial finite element software package COMSOL Multiphysics (Version5.5, COMSOL Group, Stockholm, Sweden) was used to carry out the two-dimensional numerical simulation of the designed model. The model adopts four typical built-in physical modules in COMSOL software: laminar flow, electric currents, solid mechanics and moving mesh. The accuracy and reliability of this method have been demonstrated in our previous studies, such as DEP interaction in a AC electric field (Ai et al. 2014; Zhou et al. 2020), and the electrodynamics of rigid particle in ODEP chips (Shi et al. 2020).

3 Results and discussion

3.1 The continuous separation mechanism of particles

Figure 3 shows the distribution of electric potential and electric field intensity at the initial time of particles motion. It can be seen from the figure that when the light spot irradiates the photoconductive material layer, a strong non-uniform electric field is formed near the illumination area, and the electric field intensity at the junction of the bright area and the dark area is evidently greater than that in other areas including the center area of the light spot and the area away from the light spot.

In the case that all other parameters except for particles conductivity are set uniformly, the particle motion trajectories with conductivity $\sigma_{\mathrm{P}}=4\times10^{-2}$ S/m and 4×10^{-4} S/m are given in Fig. 4A. It can be seen that when two particles are driven toward the outlet by the fluid, there is a significant y^{*}-component deviation when they move to the range $x^{*}=(-7,7)$ (Movie 1 and 2 in the Supplementary material). This is because the bright area d_{L}^{*} produced by illumination from the bottom light source is set in the range $x^{*}=(-3,3)$, which results in a strong non-uniform electric field. When the particle approaches this area, it will be subjected to different DEP actions. As shown in Fig. 4C, the particle with conductivity $\sigma_{\mathrm{P}}=4\times10^{-2}$ S/m is subjected to negative y^{*}-component of DEP force(It simply depends on the predefined axis orientation) in this area and attracted toward the area with a higher electric field intensity. Here the applied AC electric field frequency is 1 MHz, the real part of its CM factor is 0.8663

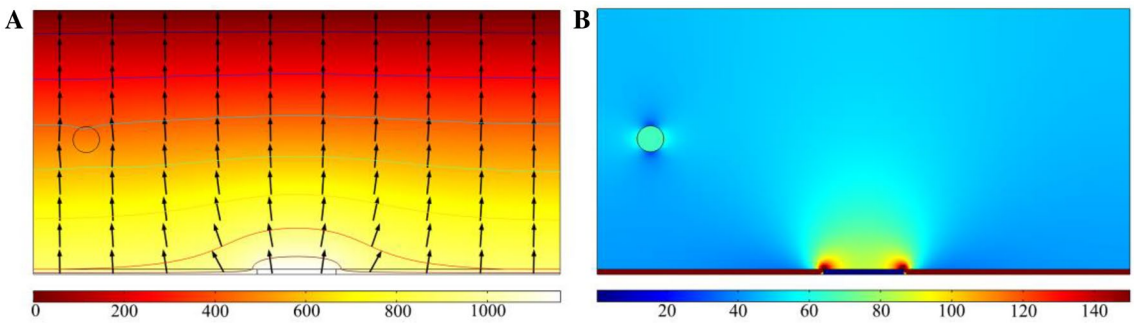

Fig. 3 The electric field distribution when the particle is located near the inlet, (A) electric potential, (B) electric field intensity. Here, the circle represents the particle, the color legend in (A) represents the electric potential, and the arrows represent the electric field direction. The color legend in (B) represents the electric field intensity

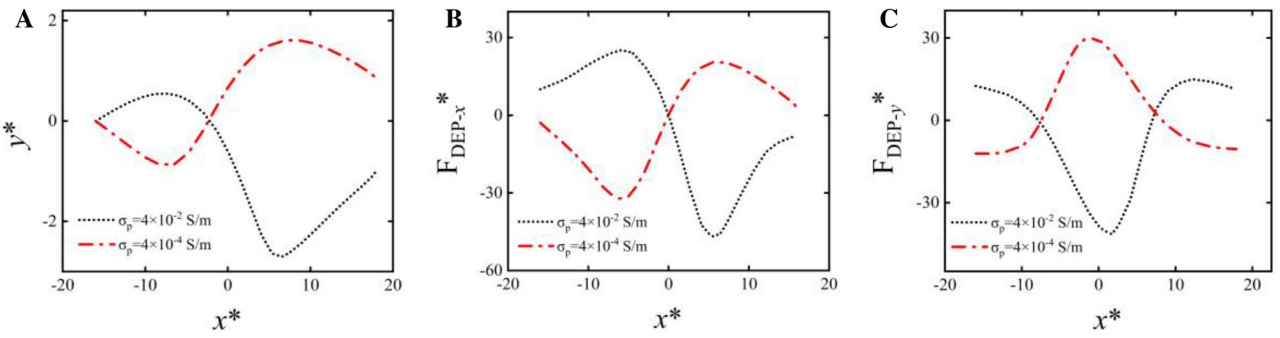

Fig. 4 The trajectories and DEP force of particles. **A** The motion trajectories of particles with conductivity (σ_P=4 × 10^{-2} S/m and 4 × 10^{-4} S/m) under the conditions of ϕ=30 V, σ_F= 1 × 10^{-3} S/m, ε_F=80 and ε_P=2.6, **B** The x*-component F^*_{DEP-x} of the DEP force depending on the particle center position x*, **C** The y*-component F^*_{DEP-y} of the DEP force depending on the particle center position x*. The initial position of the particle center located on (x^*= − 16, y^*=0) and the dimensionless particle radius a^*= 1

derived from Eqs. (1) and (2), so it can be called positive DEP action (it depends on the CM factor according to the definition of DEP action). In addition, the particle with conductivity σ_P=4 × 10^{-4} S/m is subjected to positive y*-component of DEP force in this area and repelled toward the area with a lower electric field intensity. The real part of the CM factor is − 0.4612 at the same frequency of 1 MHz, so-called negative DEP action. Therefore, due to two different DEP actions, the trajectories of particles with different conductivity are clearly differentiated, which enables the separation of particles.

Since the Reynolds number of this model is far less than 1, the fluid can be regarded as Stokes flow, and the inertial term is ignored, so the effect of inertial flow lift is not considered. It can also be seen in the supplementary material that particles at different initial positions do not exhibit y* direction migration without applying an external electric field (Movie 3 and 4 in the supplementary material). As shown in Fig. 4B, the DEP force fluctuation in the x*-component can only affect the velocity of particles through the microchannel, and it cannot compel particles to shift in the y* direction. Therefore, it can be concluded that the separation of particles with these two conductivities is mainly related to the positive and negative DEP action induced by light illumination, especially the y*-component of DEP force. It is also worth noting that before passing through x^*= − 7 and after x^*=7, the particle always presents a small y*-component deviation opposite to the direction of motion in the bright area, which could be caused by the non-uniform electric field continuously distributed in the microchannel, the DEP force of microparticle fluctuates when the particle continuously moves across the weak–strong–weak varying electric field in the microchannel. The separation effect of particles could be weakened at a certain extent, but the different trajectories of the particle can be obtained by adjusting the parameters of electric field and illumination area reasonably, thus ensuring its separation performance.

3.2 The influence of key parameters on continuous separation of particles

In addition to the conductivity of particles, other parameters, such as flow field, electric field and optical conductivity layer, can also influence the particle motion and its separation effect. The following three parameters, including the width of the bright area, the applied AC electric voltage and the flow velocity of inlet, are studied, respectively.

Figure 5 shows the dynamics of particles with three bright area widths d_L under positive and negative DEP actions according to different CM factors. As shown in Fig. 5A and D, the trajectory of particles with different widths of bright areas are compared. It can be seen that bright area width mainly affects the deflection in y*-component of the trajectory. Due to different DEP actions, the particle moves close toward or far from the bright area. The larger the bright area width is, the larger the y* direction displacement of the particle near or far from the bright area. The appropriate width of the bright area is indispensable for particles separation. If the width of the bright area is relatively small, the particle separation could not happen. Conversely, if it is excessively large, the particle would collide with one side wall, reducing the activity of the particle and resulting in poor separation performance likewise.

As shown in Fig. 5B and C, the velocity profiles of particles with different bright area widths under positive DEP action are presented. It can be seen from the velocity variation in x*-component and y*-component that the longer the width of the bright area is, the wider the action range of the DEP force. In addition, when the particle passes through the bright area, the wider bright area decelerates the movement in the x* direction and accelerates the movement in the y* direction for the positive DEP. On the contrary, as shown in Fig. 5E and F, for negative DEP, the wider bright area accelerates the movement of particles in the x* direction, which could influence the time for particles to pass through

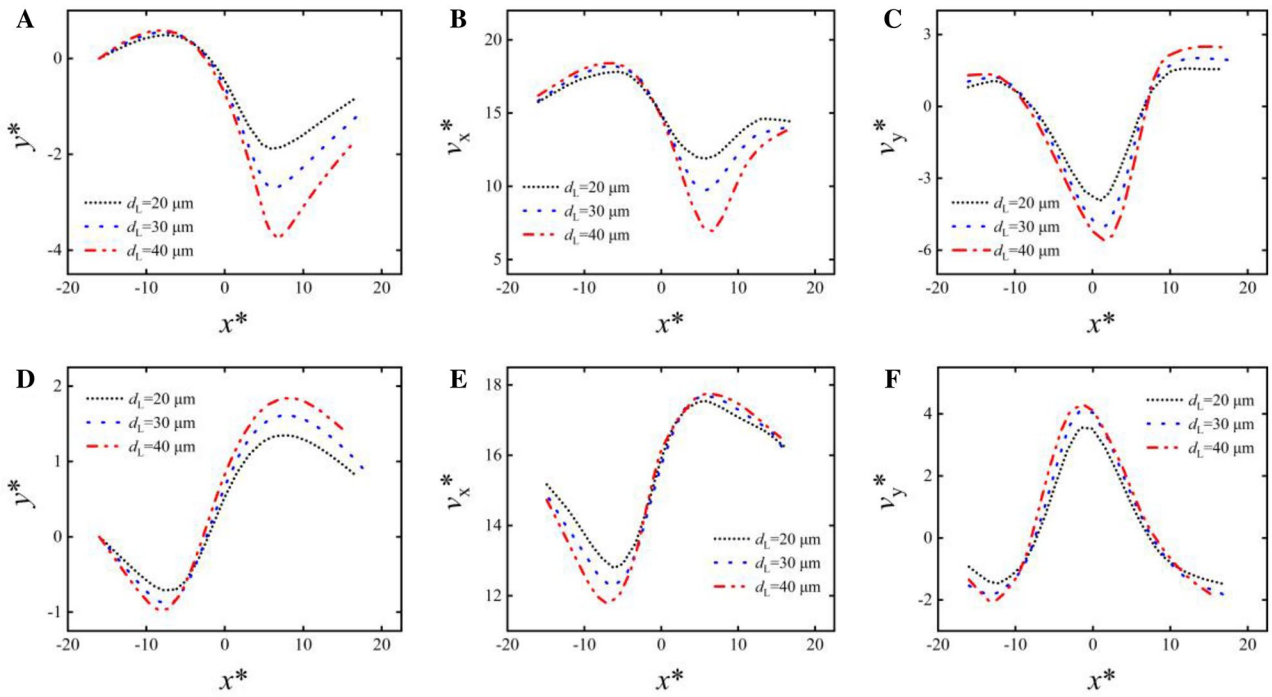

Fig. 5 The dynamics of particles at the width of bright area d_L= 20μm, 30 μm, 40 μm, ϕ=30 V and V_{inlet}=1 mm/s. The positive DEP action (with conductivity $\sigma_P=4\times10^{-2}$ S/m), **A** the motion trajectories of particles, **B** the x*-component of the particle velocity, **C** the y*-component of the particle velocity. The negative DEP action (with conductivity $\sigma_P=4\times10^{-4}$ S/m), **D** the motion trajectories of particles, **E** the x*-component of the particle velocity, **F** the y*-component of the particle velocity

the bright area. On the other hand, the wider bright area pushes particles to accelerate away from the bright area in the y* direction. It also means that not only the movement of the particle near or far away from the bright area can be controlled by adjusting the width of the bright area, but also the dwelling time of the particle across the whole microchannel can be optimized, thereby improving the particle separation efficiency.

Figure 6 shows the dynamics of particles with three applied AC electric voltages under positive and negative DEP actions according to the CM factor. As shown in Fig. 6A and D, no matter the positive DEP or the negative DEP, the particle motion trajectory can hardly be deflected in the y* direction, that is, the particle with different conductivity cannot be separated at ϕ=10 V. When the voltage rises to ϕ=20 V, the particle presents relatively different trajectories, but the separation effect is still not evident. When the voltage climbs to ϕ=30 V, the particle with different conductivity have evidently different trajectories, so a better separation performance can be achieved.

From the velocity profile of positive DEP in Fig. 6B and C, negative DEP in Fig. 6E and F, the larger the applied AC electric voltage is, the greater the fluctuation of the velocity in x* direction and y* direction. Moreover, the higher voltage results in a greater DEP force both for positive and negative DEP, which in turn generates a greater y* direction velocity and offset displacement; thus, a better separation effect is achieved. However, an exaggerated voltage could cause the particle to collide with the wall and change their trajectory disorderly in the microchannel, thus weakening the overall separation effect.

Figure 7 shows the dynamics of particles with three flow velocities of inlet under positive and negative DEP actions according to the CM factor. As shown in Fig. 7A and D, with the increase of the flow velocity, the trajectory of particles is closer to the center of the microchannel both for positive or negative DEP, and the separation effect of particles is better at a low flow velocity of inlet such as V_{inlet}=1 mm/s.

This phenomenon can be explained by the x*-component and y*-component velocities of particles with different conductivity in Fig. 7B, C, E and F. From Fig. 7B and E, it can be seen that the flow velocity of the inlet dominates the x*-component velocity of particles except for a slight change when passing through the bright area. As the flow velocity of the inlet increases, the x*-component velocity of particles increases and the particle dwelling time through the entire microchannel decreases. It can be seen from Fig. 7C and F that the flow velocity of the inlet has little influence on the y*-component velocity of particles. According to Eqs. (13) and (14), the DEP force acting on the particle is independent of the inlet flow velocity, and the liquid viscous resistance acting on the particle is tightly related to the flow velocity.

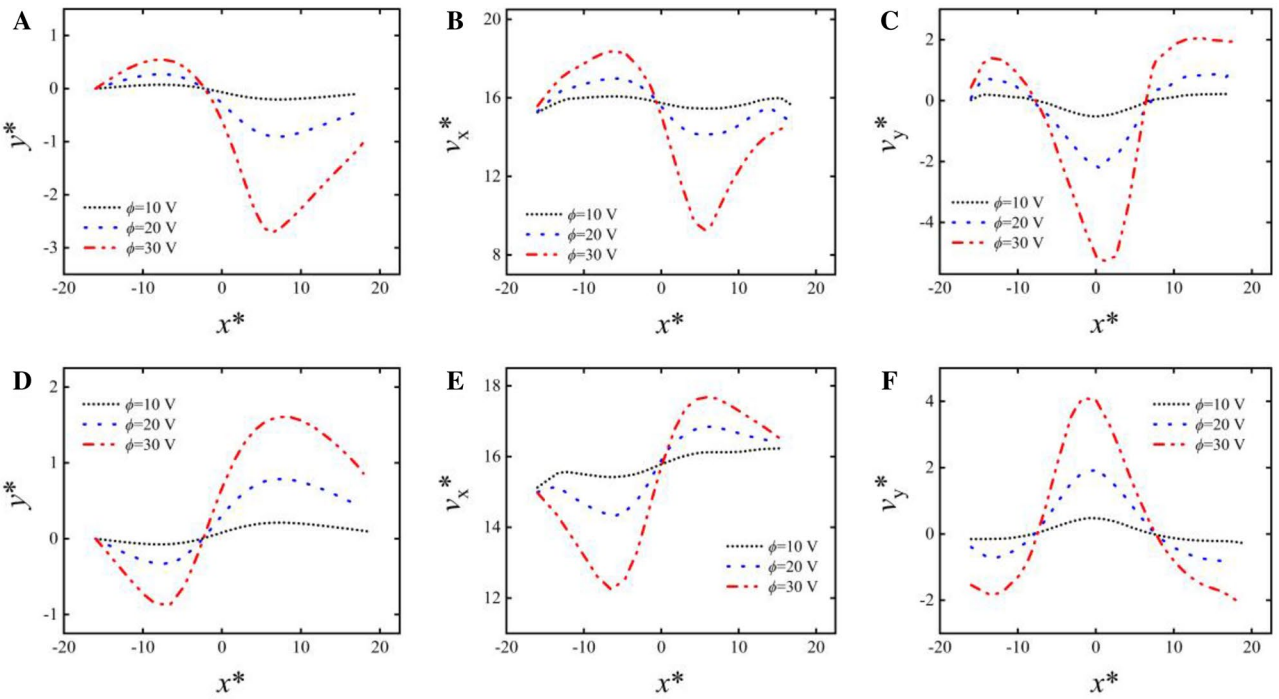

Fig. 6 The dynamics of particles with the applied AC electric voltages ϕ=10 V, 20 V, 30 V, d_L= 30μm and V_{inlet}=1 mm/s. The positive DEP action (with conductivity $\sigma_P=4\times10^{-2}$ S/m), **A** the motion trajectories of particles, **B** the x*-component of the particle velocity, **C** the y*-component of the particle velocity. The negative DEP action (with conductivity $\sigma_P=4\times10^{-4}$ S/m), **D** the motion trajectories of particle, **E** the x*-component of the particle velocity, (F) the y*-component of the particle velocity

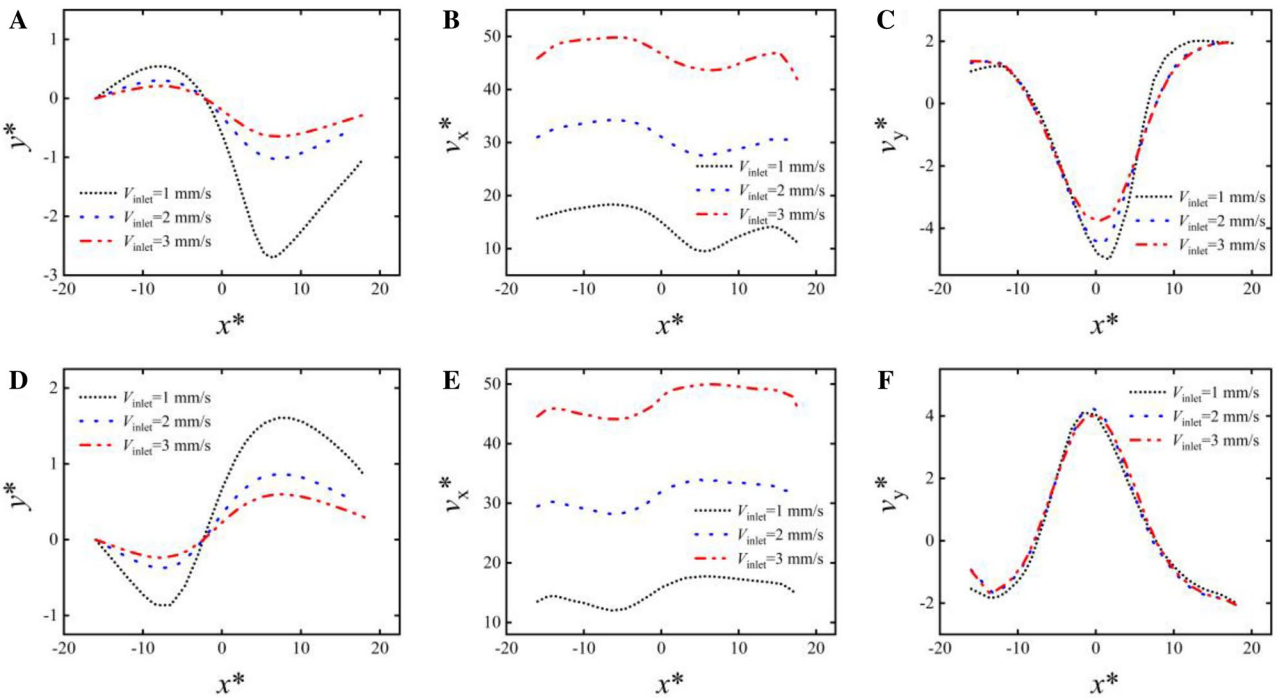

Fig. 7 The dynamics of particles at the flow velocity of inlet V_{inlet}=1 mm/s, 2 mm/s, 3 mm/s, d_L= 30μm and ϕ = 30 V. The positive DEP action (with conductivity $\sigma_P=4\times10^{-2}$ S/m), **A** the motion trajectories of particles, **B** the x*-component of the particle velocity, **C** the y*-component of the particle velocity. The negative DEP action (with conductivity $\sigma_P=4\times10^{-4}$ S/m), **D** the motion trajectories of particle, **E** the x*-component of the particle velocity, **F** the y*-component of the particle velocity

When a particle passes through the bright area, the positive or negative DEP force remains unchanged with the varying inlet flow velocity, but if the particle passes through the bright area quickly, the effective time of DEP force acting on the particle will be shortened, resulting in a smaller y^* direction offset displacement. From this point of view, the inlet flow velocity should be increased as much as possible while ensuring separation performance.

4 Conclusion

In this study, the ODEP-based transient numerical separation model containing microparticles is constructed and solved under the alternating current (AC) electric field coupling with an open flow field. The numerical results show that the separation of particles with different conductivity is dominated by the positive and negative DEP action caused by light illumination, especially the DEP force in the y-component. The continuous separation effect of particles under the combined action of AC electric field and flow field can be optimized by adjusting several key parameters. The width of the bright area affects the action range of DEP force, the applied AC electric voltage influences the magnitude of DEP force acting on particles, and the flow velocity of the inlet dominates the traveling time of particles passing through the whole microchannel, while contributing a little for particles separation. The research results clearly illuminate the basic principle of particles continuous separation and provide theoretical support for further design of particles continuous separation chip based on AC-ODEP technology in future.

Supplementary Information The online version contains supplementary material available at https://doi.org/10.1007/s10404-021-02512-0.

Acknowledgements This work is funded by National Natural Science Foundation of China (Grant No. 61964006 and No. 52075138) and Hainan Provincial Natural Science Foundation of China (Grant Nos. 519MS021 and 2019RC032).

Declarations

Conflict of interest The authors declare that they have no conflicts of interest to declare.

References

Ai Y, Qian S (2010) DC dielectrophoretic particle–particle interactions and their relative motions. J Colloid Interf Sci 346:448–454. https://doi.org/10.1016/j.jcis.2010.03.003

Ai Y, Zeng Z, Qian S (2014) Direct numerical simulation of AC dielectrophoretic particle-particle interactive motions. J Colloid Interface Sci 417:72–79. https://doi.org/10.1016/j.jcis.2013.11.034

Al Quddus N, Moussa WA, Bhattacharjee S (2008) Motion of a spherical particle in a cylindrical channel using arbitrary Lagrangian-Eulerian Method. J Colloid Interf Sci 317:620–630. https://doi.org/10.1016/j.jcis.2007.09.060

Al-Faqheri W, Thio THG, Qasaimeh MA, Dietzel A, Madou M, Al-Halhouli A (2017) Particle/cell separation on microfluidic platforms based on centrifugation effect: a review. Microfluid Nanofluid. https://doi.org/10.1007/s10404-017-1933-4

Antfolk M, Laurell T (2017) Continuous flow microfluidic separation and processing of rare cells and bioparticles found in blood—a review. Anal Chim Acta 965:9–35. https://doi.org/10.1016/j.aca.2017.02.017

Butt G, Wakeman RJ (1997) Dielectrophoresis as a capture mechanism in filtration. Jubilee Res Event 1–2:1073–1076

Chen YS, Chung KC, Huang WY, Lee WB, Fu CY, Wang CH, Lee GB (2019) Generating digital drug cocktails via optical manipulation of drug-containing particles and photo-patterning of hydrogels. Lab Chip 19:1764–1771. https://doi.org/10.1039/c9lc00189a

Chiou PY, Ohta AT, Wu MC (2005) Massively parallel manipulation of single cells and microparticles using optical images. Nature 436:370–372. https://doi.org/10.1038/nature03831

Chiu T-K et al (2018) Optically-induced-dielectrophoresis (ODEP)-based cell manipulation in a microfluidic system for high-purity isolation of integral circulating tumor cell (CTC) clusters based on their size characteristics. Sens Actuat B 258:1161–1173. https://doi.org/10.1016/j.snb.2017.12.003

Chu PY, Liao CJ, Hsieh CH, Wang HM, Chou WP, Chen PH, Wu MH (2019) Utilization of optically induced dielectrophoresis in a microfluidic system for sorting and isolation of cells with varied degree of viability: demonstration of the sorting and isolation of drug-treated cancer cells with various degrees of anti-cancer drug resistance gene expression. Sens Actuat B 283:621–631. https://doi.org/10.1016/j.snb.2018.12.047

Chu PY, Hsieh CH, Lin CR, Wu MH (2020) The effect of optically induced dielectrophoresis (ODEP)-based cell manipulation in a microfluidic system on the properties of biological cells. Biosensors (basel). https://doi.org/10.3390/bios10060065

Galbraith D (2012) Flow cytometry and cell sorting: the next generation. Methods 57:249–250. https://doi.org/10.1016/j.ymeth.2012.08.010

Heinlaan M, Muna M, Juganson K, Oriekhova O, Stoll S, Kahru A, Slaveykova VI (2017) Exposure to sublethal concentrations of Co_3O_4 and Mn_2O_3 nanoparticles induced elevated metal body burden in Daphnia magna. Aquat Toxicol 189:123–133. https://doi.org/10.1016/j.aquatox.2017.06.002

Hu HH, Patankar NA, Zhu MY (2001) Direct numerical simulations of fluid-solid systems using the arbitrary lagrangian-eulerian technique. J Comput Phys 169:427–462. https://doi.org/10.1006/jcph.2000.6592

Liang WF, Liu N, Dong ZL, Liu LQ, Mai JD, Lee GB, Li WJ (2013) Simultaneous separation and concentration of micro- and nanoparticles by optically induced electrokinetics. Sens Actuat A 193:103–111. https://doi.org/10.1016/j.sna.2013.01.020

Lin ZT, Lin SY, Xie PF, Lin CY, Rather GM, Bertino JR, Javanmard M (2020) Rapid assessment of surface markers on cancer cells using immuno-magnetic separation and multi-frequency impedance cytometry for targeted therapy. Sci Rep-UK. https://doi.org/10.1038/s41598-020-57540-7

Pethig R, Markx GH (1997) Applications of dielectrophoresis in biotechnology. Trends Biotechnol 15:426–432. https://doi.org/10.1016/S0167-7799(97)01096-2

Porter J, Edwards C, Morgan JA, Pickup RW (1993) Rapid, automated separation of specific bacteria from lake water and sewage by flow cytometry and cell sorting. Appl Environ Microb 59:3327–3333. https://doi.org/10.1128/aem.59.10.3327-3333.1993

Qu YL, Zheng MJ, Liang WF, Dong ZL (2012) Fully automatic wafer-scale micro/nano manipulation based on optically induced

dielectrophoresis. Adv Mater Res-Switz 415–417:842–847. https://doi.org/10.4028/www.scientific.net/AMR.415-417.842

Shi L, Shi X, Zhou T, Liu Z, Liu Z, Joo S (2020) A full-scale computational study on the electrodynamics of a rigid particle in an optically induced dielectrophoresis chip. Modern Phys Lett B. https://doi.org/10.1142/s0217984920502334

Shields CW, Reyes CD, Lopez GP (2015) Microfluidic cell sorting: a review of the advances in the separation of cells from debulking to rare cell isolation. Lab Chip 15:1230–1249. https://doi.org/10.1039/c4lc01246a

Tsou PH, Chiang PH, Lin ZT, Yang HC, Song HL, Li BR (2020) Rapid purification of lung cancer cells in pleural effusion through spiral microfluidic channels for diagnosis improvement. Lab Chip 20:4007–4015. https://doi.org/10.1039/d0lc00663g

Wang X, Wang X-B, Gascoyne PRC (1997) General expressions for dielectrophoretic force and electrorotational torque derived using the maxwell stress tensor method. J Electrostat 39:277–295. https://doi.org/10.1016/S0304-3886(97)00126-5

Wang H-Y, Chen C-Y, Chu P-Y, Zhu Y-X, Hsieh C-H, Lu J-J, Wu M-H (2020) Application of an optically induced dielectrophoresis (ODEP)-based microfluidic system for the detection and isolation of bacteria with heterogeneity of antibiotic susceptibility. Sens Actuat B. https://doi.org/10.1016/j.snb.2019.127540

Xie SX, Wang XD, Jiao ND, Tung S, Liu LQ (2017) Programmable micrometer-sized motor array based on live cells. Lab Chip 17:2046–2053. https://doi.org/10.1039/c7lc00017k

Yan B, Chen B, Liu FY, Wu JK, Xiong YL (2021) Combining field-modulating electroosmotic vortex and insulating post to manipulate particles based on dielectrophoresis. Appl Math Mech-Engl. https://doi.org/10.1007/s10483-021-2706-5

Zhao Y, Hu S, Wang Q (2014a) Simulation and analysis of particle trajectory caused by the optical-induced dielectrophoresis force. Microfluid Nanofluid 16:533–540. https://doi.org/10.1007/s10404-013-1246-1

Zhao Y, Hu S, Wang Q (2014b) Study on the assembly and separation of biological cell by optically induced dielectrophoretic technology. Microfluid Nanofluid 17:287–294. https://doi.org/10.1007/s10404-013-1311-9

Zhou T, Ji X, Shi L, Zhang X, Song Y, Joo SW (2020) AC dielectrophoretic deformable particle-particle interactions and their relative motions. Electrophoresis 41:952–958. https://doi.org/10.1002/elps.201900266